Full field of view point spread function for circular synthetic aperture sonar systems

Yan Pailhas, Yvan Petillot, and Bernard Mulgrew

Citation: Proc. Mtgs. Acoust. **30**, 005003 (2017);
View online: https://doi.org/10.1121/2.0000585
View Table of Contents: http://asa.scitation.org/toc/pma/30/1
Published by the Acoustical Society of America

Proceedings of Meetings on Acoustics

Volume 30 http://acousticalsociety.org/

Acoustics `17 Boston

173rd Meeting of Acoustical Society of America and 8th Forum Acusticum
Boston, Massachusetts
25-29 June 2017

Acoustical Oceanography: Paper 5aAO4

Full field of view point spread function for circular synthetic aperture sonar systems

Yan Pailhas
School of Engineering and Physical Sciences, Heriot-Watt University, Edinburgh, Scotland, EH14 4AS, UNITED KINGDOM; Y.Pailhas@hw.ac.uk

Yvan Petillot and Bernard Mulgrew
Heriot-Watt University, Edinburgh, Scotland,UNITED KINGDOM; Y.R.Petillot@hw.ac.uk; Bernie.Mulgrew@ed.ac.uk

The introduction of SAS (Synthetic Aperture Sonar) systems has been a game changer for underwater surveys. The gain in resolution, compared to traditional sidescan systems, created a paradigm shift as the information contained in a SAS image switches from shadows to highlights. SAS systems traditionally perform lawnmower type surveys, but the need for multiple views in MCM (Mine-Counter Measure) tasks, for example, opened the interesting problem of target re-acquisition patterns. In particular, circular patterns maximize the aperture, thus the overall image resolution of such system. The capability of CSAS (Circular SAS) has been demonstrated on the field, but the derivation of CSAS processing has not been fully developed. The non-uniform sampling of the circular pattern in particular introduces aberrations within the field of view and a non uniform PSF (Point Spread Function). We propose a spatial sampling scheme which makes the CSAS PSF perfectly uniform and keeps a constant SNR (Signal-to-Noise Ratio). We also derive analytically the CSAS PSF for offset points.

Published by the Acoustical Society of America

 https://doi.org/10.1121/2.0000585

1. INTRODUCTION

SAS (Synthetic Aperture Sonar) and SAR (Synthetic Aperture Radar) share the same fundamental principles: process coherently multiple acquisitions to form a large synthetic antenna. The output of coherent processing is a very high resolution image. The required precision for the antenna location to enable coherent processing is estimated at around $\lambda/8$, where λ represents the wavelength. This specific problem has been proven to be particularly challenging for the underwater community. The micro-navigation problem has been solved by Bellettini in[1] thanks to the DPCA (Displaced Phase Centre Antenna) algorithm. SAS has been a game changer for the community. For example, the increased resolution compared to more traditional systems has made ATR (Automatic Target Recognition) algorithms more reliable.[2–4] In recent years, new acquisition and re-acquisition patterns have emerged, in particular circular SAS acquisition also known as CSAS. CSAR (Circular SAR) has been studied for few decades already[5,6] for various applications, and the SAR community showed the great potential of such system. CSAS offers some challenges in term of feasibility[7] or image processing[8,9] and has not been fully investigated yet. The problem of the PSF (Point Spread Function) of such system in particular remains. In[10] , we derived the analytical expression of the CSAS PSF for the central point, and proposed a resampling scheme to make the PSF uniform everywhere within the full view area. The PSF problem raises the fundamental question of CSAS image formation and is essential to develop any image improvement algorithm. In this paper, we extend the results from[10] and bring two main contributions:

- We derive in section 4.2 the analytical expression of the CSAS PSF for any point within the full view area. Although a direct derivation is not trackable, we use a wavelet analysis to derive the exact PSF expression. Numerical simulations validating our approach are also presented.
- We propose a new method to make the PSF uniform. The PSF uniformisation is presented in section 2 and is based on a refined resampling scheme which solves the problem of the non uniformity of the SNR (Signal-to-Noise Ratio).

The paper is organised as follows: In section 2, we describe the configuration and notations related to a CSAS system. We also derive the first resampling scheme and solve the SNR dependency problem. In section 3, we calculate the analytical expression of the matched filter response. Section 4 is dedicated to the PSF problem, we recall the PSF expression for the central point in section 4.1 before extending the PSF calculation to an offset point in section 4.2.

2. CSAS CONFIGURATION

We consider a SAS system **S** performing a circle $\mathcal{C}$ centred in **O** and with a radius R. The full view area is described as the area where each point is insonified by **S** during the full revolution. Assuming that the trajectory is a circle, the full view area as also a circle centred in **O** whose radius $\mathrm{R_{FV}}$ is function of R and the SAS beamwidth φ, $\mathrm{R_{FV}} = \mathrm{R}\sin(\varphi/2)$. Figure 1 pictures the geometry of the problem. The full view area is highlighted in blue.

Considering now the point **O'** within the full view area. The distance **OO'** can be written as $\alpha\mathrm{R}$ where $\alpha \le \sin(\varphi/2)$. When the system **S** is in A, it has traveled $\theta\mathrm{R}$ from it original position, but it sees the point **O'** at an angle θ'. The two angles θ and θ' are linked through the following set of equations

$$\theta' = h(\theta) = \mathrm{sgn}(\theta)\cos^{-1}\left(\frac{\cos\theta - \alpha}{\sqrt{1+\alpha^2-2\alpha\cos\theta}}\right) \text{ and} \tag{1}$$

$$\theta = h^{-1}(\theta') = \mathrm{sgn}(\theta')\cos^{-1}\left(\alpha\sin^2\theta' + \cos\theta'\sqrt{1-\alpha^2\sin^2\theta'}\right). \tag{2}$$

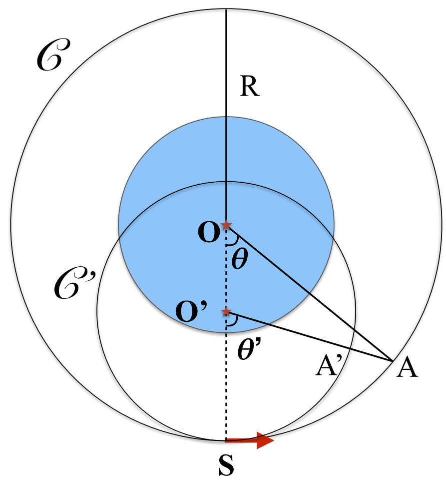

Figure 1: Isomorphism between the real SAS trajectory, $\mathcal{C}$, and virtual trajectory, $\mathcal{C}'$.* S *represents the location of the SAS system following the circular trajectory $\mathcal{C}$. The full view area is highlighted in blue.

Note that the relationship between θ and θ' is not linear. A direct consequence is that the integration along $\mathcal{C}$ is not uniform for **O'**. Thus, the PSF is not uniform within the full view area, as we will see in section 4. In[10] we propose a sampling scheme to make uniform the PSF. The integration for the point **O'** can be done by integrating along $\mathcal{C}'$ instead of $\mathcal{C}$ by putting

$$\theta'_n = n\frac{\delta\theta}{(1-\alpha)R} \tag{3}$$

into Eq. (2). The summation is then done on the subset $\{\theta_n\}_n$, where $\theta_n = \mathrm{NN}(h^{-1}(\theta'_n))$, where $\mathrm{NN}(.)$ represents the Nearest Neighbour operator. The integration will then be uniformly sampled, at regular interval $\delta\theta$, along $\mathcal{C}'$. This method has one drawback however: the non-uniform downsampling of the angle of integration θ slightly decreases the SNR (Signal-to-Noise Ratio) as the resampling gets away from the centre **O**.

This inconvenience can be easily corrected by modifying the summation scheme. Assuming a point scatterer in **O'**, the response of **O'** after CSAS processing is described mathematically by:

$$I(\mathbf{O}') = \int_{\mathcal{C}} s^{\tau}_{\mathrm{MF}}(t)d\tau, \tag{4}$$

where $s^{\tau}_{\mathrm{MF}}(t)$ is the matched filter echo received at the slow time τ. Note that the slow time is linked linearly to the position θ of the system along $\mathcal{C}$. In practice, the acquisition is discrete and (4) rewrites as

$$I(\mathbf{O}') = \sum_{n=1}^{N} s^{\theta_n}_{\mathrm{MF}}(t). \tag{5}$$

The resampling scheme suggested by (3) is then

$$I(\mathbf{O}') = \sum_{n=1}^{N'} s^{\mathrm{NN}(h^{-1}(\theta'_n))}_{\mathrm{MF}}(t). \tag{6}$$

The SNR diminishes because $N' < N$. To keep a constant SNR, we first divide the set of all the acquisition angle $\{\theta_n\}_{n\in[1,N]}$ into the set of subsets

$$\{\theta_n\}_{n\in[1,N]} = \left\{\{\theta^k_{n'}\}_{k\in[1,K_{n'}]}\right\}_{n'\in[1,N']}, \tag{7}$$

where $\theta^k_{n'}$ is such as $\mathrm{NN}(h(\theta^k_{n'}) = \theta'_n$ with θ'_n given by (3). The integration (5) then can be computed as

$$I(\mathbf{O}') = \sum_{n'=1}^{N'} \frac{1}{K_{n'}} \sum_{k=1}^{K_{n'}} s^{\theta^k_{n'}}_{\mathrm{MF}}(t). \tag{8}$$

Because the summation in (8) is performed on all the original acquisitions $\{\theta_n\}_n$, the SNR is uniform for all the full view area. The clustering of the $\theta^k_{n'}$ ensures the uniform angular sampling of Eq. (4) for every points within the full field of view.

For the rest of the paper, we will be using the nomenclature described in Table 1 for the central frequency, the bandwidth, the pulse length and the Gaussian window temporal length related to the pulse. For the numerical simulations and unless otherwise specified, we will be using the values also indicated in Table 1.

Notations	Definition	Values	Units
c	sound speed	1500	m.s^{-1}
f_0	pulse centre frequency	100	kHz
Δf	bandwidth	20	kHz
T	pulse length	1	ms
σ	Gaussian window temporal width	200	µs

Table 1: Nomenclature and nominal values.

3. THE MATCHED FILTER RESPONSE

In this section, we compute the matched filter response of a linear frequency modulated (LFM) signal weighted by a rectangular window and a Gaussian window. The matched filter response solves the range compression problem and plays an important role in the derivation of the PSF.

Let $p(t)$ the pulse sending by the SAS system. We assume that $p(t)$ is a weighted LFM signal. Thus, we can write:

$$p(t) = W(t)\exp\left[2i\pi\left(f_0 + \frac{\Delta f}{2T}t\right)t\right], \tag{9}$$

where $W(t)$ is the windowing function. We are considering two cases for $W(t)$, a rectangular window:

$$W(t) = \mathbb{1}_{[-T/2,T/2]}(t), \tag{10}$$

and a Gaussian window:

$$W(t) = \exp\left(-\frac{t^2}{2\sigma^2}\right). \tag{11}$$

The matched filter response $s_{\mathrm{MF}}(t)$ of the pulse (9) is given by:

$$\begin{aligned} p_{\mathrm{MF}}(t) &= \int_{-\infty}^{+\infty} p^*(t')p(t'+t)\,\mathrm{d}t' \\ &= e^{2i\pi\left(f_0+\frac{\Delta f}{2T}t\right)t}\int_{-\infty}^{+\infty} W(t')W(t'+t)\exp\left[2i\pi\frac{\Delta f}{T}t't\right]\,\mathrm{d}t' \end{aligned} \tag{12}$$

The exact analytic expression of the matched filter response (12) can be found for both windowing functions (10) and (11) as described in[11] and[10] respectively, and $p_{\mathrm{MF}}(t)$ reduces to

$$p_{\mathrm{MF}}(t) = B(t)\,e^{2i\pi f_0 t}, \tag{13}$$

with

$$\begin{aligned} B(t) &= T\tfrac{\sin[\pi t\Delta f(1-|t|/T)]}{\pi t\Delta f} && \text{for the rectangular windowing (10) and} && (14)\\ &= \sigma\sqrt{\pi}\exp\left[-\left(\tfrac{1}{4\sigma^2}+\pi^2\tfrac{\Delta f^2}{T^2}\sigma^2\right)t^2\right] && \text{for the Gaussian windowing (11).} && (15) \end{aligned}$$

From (13), it is interesting to note that the matched filter response $p_{\mathrm{MF}}(t)$ is only a low frequency envelope, $B(t)$, modulated by the central frequency f_0. The frequency content of $p_{\mathrm{MF}}(t)$ then comes from the frequency leakage caused by the windowing function $B(t)$.

4. THE PSF PROBLEM

The PSF plays a central role in the understanding of the resolution problem. It is in essence the founding pillar of the image formation. In this section, we derive analytically the CSAS PSF at first for the central point and then we extend the derivation to any offset point in the full view area.

A. CENTRE POINT PSF

To recover the CSAS PSF, we need to integrate the received echoes along the full circular trajectory $\mathcal{C}$. We consider an ideal scatterer located at the centre **O** of the circle $\mathcal{C}$. Given the circular geometry of the problem, it is convenient to compute the PSF is the polar coordinates where **O** represents the origin. Furthermore, the PSF $I(r,\theta)$ is only function of r, the distance to the centre **O**, *i.e.* $I(r,\theta) = I(r)$. The integration along $\mathcal{C}$ gives the PSF, and we can write

$$I(r) = \int_{\theta=0}^{2\pi} B\left(\frac{2r\cos\theta}{c}\right)e^{4i\pi f_0 r\cos\theta/c}\,\mathrm{d}\theta. \tag{16}$$

Using a first order approximation of the MacLaurin series for $B(.)$ leads to the PSF expression for CSAS configuration:

$$I(r) = 2\pi B\left(\frac{2r}{c}\right)J_0(2kr) \tag{17}$$

with $k = 2\pi f_0/c$ representing the wave number and $J_0(.)$ the Bessel function of the first kind of order 0.

In figure 2(a), we plot the PSF as a function of r and compare the exact solution (16) with the approximation given by (17). The numerical simulation has been performed using the numerical value given in Table 1. The close match between the two curves indicates that the first order approximation reflects accurately the circular integration. Figure 2(b) draws the 2D normalised CSAS PSF for a pulse with a Gaussian windowing.

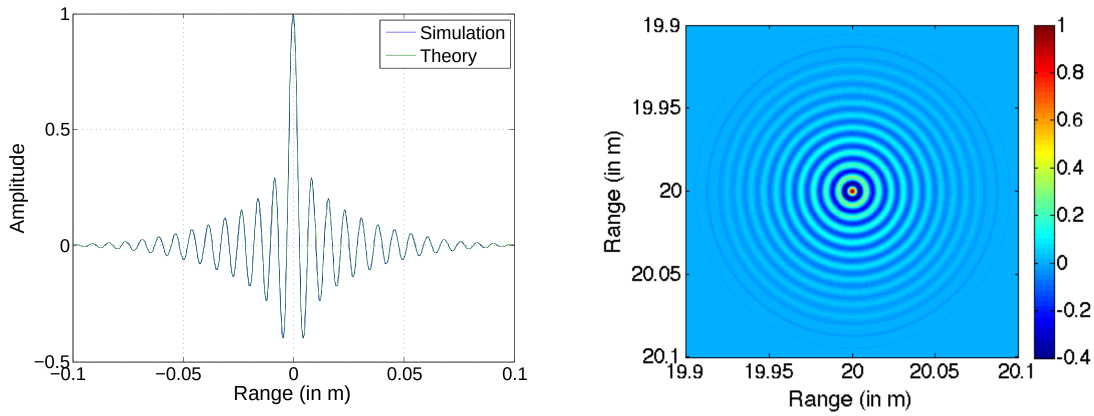

(a) (b)

Figure 2: (a) Comparison between the full SAS integration from Eq. (16) ***and the approximation from Eq.*** (17) ***for a pulse with a Gaussian windowing. (b) Normalised PSF for a CSAS system using a pulse with a Gaussian window.***

B. OFFSET POINT PSF

In section 4.1, we give the analytical expression of the CSAS response of the centre point. In this section, we will compute the PSF for every point within the field of view given by the system. But to do so, we need first to understand and then compute the CSAS PSF (17) in the Fourier domain.

The Fourier transform $\hat{I}(\rho,\phi)$ of the function $I(r,\theta)$ in polar coordinates is given by:

$$\hat{I}(\rho,\phi) = \int_{r=0}^{+\infty} \int_{\theta=0}^{2\pi} I(r,\theta) e^{2i\pi\rho r \cos(\theta-\phi)} r \,\mathrm{d}r\mathrm{d}\theta \tag{18}$$

In our case, we already saw that, thanks to the circular symmetry, $I(r,\theta)$ reduces to $I(r)$. Thus, $\hat{I}(\rho,\phi) = \hat{I}(\rho)$ and (18) can be simplified as

$$\hat{I}(\rho) = 2\pi \int_{r=0}^{+\infty} I(r) J_0(2\pi r\rho) r \,\mathrm{d}r, \tag{19}$$

where $J_0(.)$, as before, represents the Bessel function of the first kind of order 0. Using the expression (17) for the Gaussian windowing case into (19) gives :

$$\hat{I}(\rho) = 8\pi^{5/2}\sigma a_0^2 \int_{r=0}^{+\infty} \exp(-r^2) J_0(2\sqrt{2}ka_0 r) J_0(2\sqrt{2}\pi a_0 \rho r) r \,\mathrm{d}r, \tag{20}$$

where $a_0 = \frac{1}{\sqrt{2}} \frac{c\sigma T}{\sqrt{T^2+4\pi^2\Delta f^2\sigma^4}}$ and k is the wave number $\frac{2\pi f_0}{c}$. The analytical solution of (20) is given by the generalisation of the Weber's second exponential integral[12] :

$$\hat{I}(\rho) = 4\pi^{5/2}\sigma a_0^2 I_0(4\pi k a_0^2 \rho) \exp\left[-2a_0^2(k^2+\pi^2\rho^2)\right]. \tag{21}$$

where $I_0(.)$ is the modified Bessel function of the first kind. The physical interpretation of (21) is challenging. However, by using the fact that for most systems the quality factor $Q > 2$ which justifies the asymptotic derivation of the Bessel function $I_0(.)$, (21) rewrites as[10] :

$$\hat{I}(\rho) \approx 2\pi^{3/2} \frac{\sigma a_0}{\sqrt{2k\rho}} \exp\left[-2a_0^2(\pi\rho - k)^2\right]. \tag{22}$$

Equation (22) further simplifies to:

$$\hat{I}(\rho) \approx \sqrt{2}\pi^2 \frac{\sigma a_0}{k} \exp\left[-2a_0^2(\pi\rho - k)^2\right], \tag{23}$$

using the same constraint on the quality factor. Unlike (21), the interpretation of (22) is straightforward: in the Fourier domain, the CSAS PSF is then a Gaussian ring with a diameter of $2f_0/c$ and a variance of $1/\pi^2 a_0^2$. Figure 3 draws the normalised CSAS PSF at the centre of $\mathcal{C}$ in the Fourier domain.

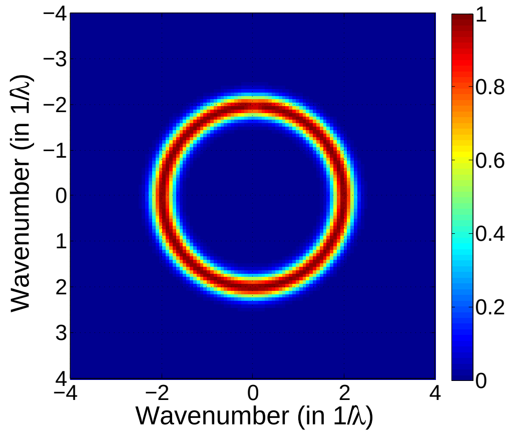

***Figure 3: Normalised 2D Fourier transform for a perfect scattering point target located in the origin* O.**

Direct analytical derivation of (4) for the full view area is not feasible. To compute the CSAS PSF in every points in the full view area, we will first made a plane wave hypothesis. Considering one ideal scatterer located in **O'**(x_0, y_0) and under the plane wave assumption (4) rewrites in the Cartesian coordinates:

$$I(x,y) = \int_{\mathcal{C}} B\left(2\frac{(x-x_0)\cos\theta' - (y-y_0)\sin\theta'}{c}\right) \exp ik((x-x_0)\cos\theta' - (y-y_0)\sin\theta')d\theta. \tag{24}$$

Before developing further, we need to demonstrate the equivalence between (24) and (4). For the readability of the equations, we will omit from now on the x_0 and y_0 dependency. Let

$$\psi(x,y,\theta') = B\left(2\frac{x\cos\theta' - y\sin\theta'}{c}\right) \exp ik(x\cos\theta' - y\sin\theta') \tag{25}$$

be the integrand of (24). Following the same method used to calculate $\hat{I}(\rho)$ and after tedious calculations, we find that the 2D Fourier transform of $\psi(x,y,\theta')$ relative to (x,y) is:

$$\hat{\psi}(\rho,\phi,\theta') = \sqrt{2}\pi\sigma a_0 \exp\left[-2a_0^2(\pi\rho - k)^2\right]\delta(\phi + \theta' + \pi/2). \tag{26}$$

Note that the result is not surprising: the Dirac function $\delta(.)$ came from the $\exp(.)$ expression in (25) and the Gaussian window from the $B(.)$ term we already computed earlier. Of course, the choice in the notations was not innocent: $\{\hat{\psi}\}_{\theta'}$ is in essence a wavelet basis which reconstructs exactly the PSF (24). This demonstrates that (24) is consistent with the original formulation (4). We can now operate a change of variable in (24) as described below:

$$\begin{aligned} \hat{I}(\rho,\phi) &= \int_{\theta=-\pi}^{+\pi} \hat{\psi}(\rho,\phi,\theta')d\theta \\ &= \int_{\theta'=-\pi}^{+\pi} \hat{\psi}(\rho,\phi,\theta')\frac{\mathrm{d}h^{-1}(\theta')}{\mathrm{d}\theta'}d\theta' \end{aligned} \tag{27}$$

where

$$\frac{\mathrm{d}h^{-1}(\theta')}{\mathrm{d}\theta'} = g(\theta') = \frac{\sin\theta'\sqrt{1-\alpha^2\sin^2\theta'} + \frac{\alpha^2\cos^2\theta'\sin^2\theta'}{\sqrt{1-\alpha^2\sin^2\theta'}} - 2\alpha\cos\theta'\sin\theta'}{\sqrt{1-\left(\cos\theta'\sqrt{1-\alpha^2\sin^2\theta'}+\alpha\sin^2\theta'\right)^2}} \tag{28}$$

It is interesting to note that the first order of the MacLaurin series of (28) reduces to:

$$g(\theta') = 1 - \alpha\cos\theta' + \mathcal{O}(\alpha^2). \tag{29}$$

Numerical simulations show that the first order approximation given by (29) is a great fit for $\alpha \leq \frac{1}{2}$. Finally, by putting (26) into (27), we arrive to the CSAS PSF for an offset point in the Fourier domain:

$$\hat{I}(\rho,\phi) = 2\pi^{3/2}\frac{\sigma a_0}{\sqrt{2k\rho}}\exp\left[-2a_0^2(\pi\rho-k)^2\right]g(\phi+\theta_0+\pi/2) \tag{30}$$

where θ_0 is the angular coordinate of **O'** in polar coordinates. Comparing the PSF for an offset point given by (30) and the central point (22), we observe that the two expressions only differ by the angular weighting factor $g(\phi+\theta_0+\pi/2)$. Figure 4(a) plots a 3D representation of the spectral CSAS PSF for an offset point with the parameters $\alpha = \frac{1}{\sqrt{2}}$ and $\theta_0 = 45°$ computed directly from Eq. (4). As expected, the PSF in the Fourier domain is no longer symmetric and there is a strong angular dependency.

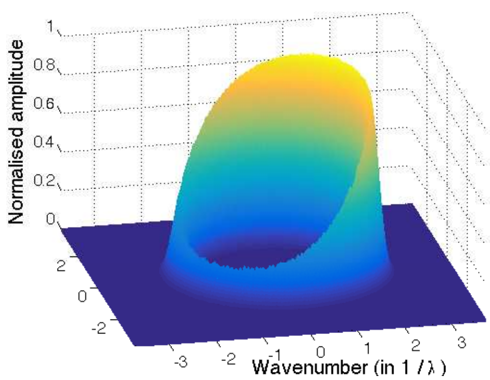

(a)

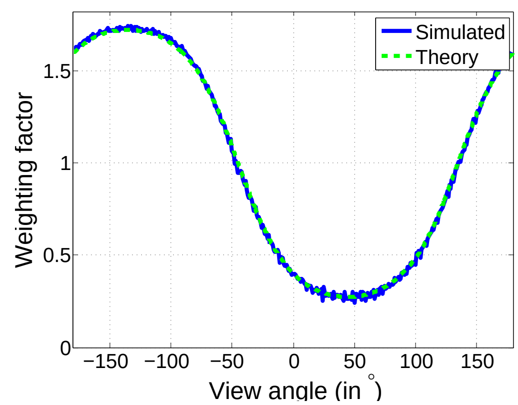

(b)

***Figure 4:** (a) 3D plot of the normalised Fourier transform of an offset point. (b) Angular weighting factor for simulated data and the one given by* (30)*.*

In figure 4(b), we compare the angular weighting coefficient between the simulated data plotted in figure 4(a) and the theoretical value $g(.)$ from Eq. (28). We obtain a perfect match between the two curves minus the noise from the simulation.

5. CONCLUSIONS

In this paper we derived an analytic expression for the point spread function relative to a fully coherent CSAS for every points within the full field of view. Although a direct calculation is not trackable, we used wavelet analysis to obtain the PSF expression. The PSF of an offset point differs from the PSF of the central by an angular weighted factor analytically trackable. In future works, we aim to test our algorithm on real CSAS data.

ACKNOWLEDGMENTS

This work was supported by the Engineering and Physical Sciences Research Council (EPSRC) Grant number EP/J015180/1 and the MOD University Defence Research Collaboration in Signal Processing.

REFERENCES

[1] A. Bellettini and M. A. Pinto. Theoretical accuracy of synthetic aperture sonar micronavigation using a displaced phase-center antenna. *IEEE Journal of Oceanic Engineering*, 27(4):780–789, Oct 2002.

[2] Y. Pailhas, Y. Petillot, and C. Capus. High-resolution sonars: What resolution do we need for target recognition? *EURASIP Journal on Advances in Signal Processing*, 2010(1):205095, 2010.

[3] J. Sawas, Y. Petillot, and Y. Pailhas. Cascade of boosted classifiers for rapid detection of underwater objects. In *Proceedings of the European Conference on Underwater Acoustics*, pages 1507–1516. Institute of Acoustics, St Alban, UK, 2010.

[4] V. Myers and J. Fawcett. A template matching procedure for automatic target recognition in synthetic aperture sonar imagery. *IEEE Signal Processing Letters*, 17(7):683–686, 2010.

[5] M. Soumekh. Reconnaissance with slant plane circular SAR imaging. *IEEE Transactions on Image Processing*, 5(8):1252–1265, Aug 1996.

[6] T.-K. Chan, Y. Kuga, and A. Ishimaru. Experimental studies on circular sar imaging in clutter using angular correlation function technique. *IEEE Transactions on Geoscience and Remote Sensing*, 37(5):2192–2197, Sep 1999.

[7] B. G. Ferguson and R. J. Wyber. Application of acoustic reflection tomography to sonar imaging. *The Journal of the Acoustical Society of America*, 117(5):2915–2928, 2005.

[8] T. M. Marston, J. L. Kennedy, and P. L. Marston. Autofocusing circular synthetic aperture sonar imagery using phase corrections modeled as generalized cones. *The Journal of the Acoustical Society of America*, 136(2):614–622, 2014.

[9] Daniel S. Plotnick, Philip L. Marston, and Timothy M. Marston. Fast nearfield to farfield conversion algorithm for circular synthetic aperture sonar. *The Journal of the Acoustical Society of America*, 136(2):EL61–EL66, 2014.

[10] Y. Pailhas, Y. Petillot, and B. Mulgrew. Increasing circular synthetic aperture sonar resolution via adapted wave atoms deconvolution. *J. Acoust. Soc. Am.*, 141(4):2623–2632, 2017.

[11] M. Cheney and B. Borden. *Fundamentals of Radar Imaging*. pp. 149. Society for Industrial and Applied Mathematics, Philadelphia, US, 2008.

[12] G. N. Watson. *Theory of Bessel functions*. pp. 805. Cambridge University Press., Cambridge, UK, 1966.